Section S1 – Observed dataset and instrumentation

Table S1 summarizes the measured variables, instruments, and associated uncertainties used in the green roof monitoring campaign.

Table S1: Measured variables and their respective instruments used in monitoring the London experimental green roof.

Variable	Instrument	Error	Data Use
Air temperature	T&RH HC3-S3	0.5 °C	Input forcing, energy fluxes calculations
Relative humidity		1.5%	Input forcing, energy fluxes calculations
Net radiation	Net Radiometer REBS Q7.1	8%	Energy fluxes calculations
Incoming longwave radiation	Pyrgeometer Eppley PIR	5 W m^{-2}	Input forcing
Incoming solar radiation	Pyranometer YES TSP-400	10%	Input forcing
Reflected solar radiation			Microclimate context
Green roof surface temperature	IRT Apogee SI-121	0.2 °C	Model evaluation
Subsurface temperature (at 2.54 cm and 10.16 cm)	3 junction averaging thermocouples Omega Type T	0.5 °C	Energy fluxes calculations
Wind speed and direction	Anemometer/Wind vane R.M Young 3102 Wind Sentry Set	0.5 m s^{-1}	Input forcing
Drainage	Custom drainage unit based on a tipping bucket rain gauge	1%	Energy fluxes calculations

Precipitation	Rain Gauge Texas Electronics Tipping bucket TE525WS	1%	Input forcing, energy fluxes calculations
Module weight change	Custom lysimeter based on an Interface Load Cell	0.0054 kg	Energy fluxes calculations
Soil heat flux (at 7 cm)	Campbell Scientific HFP01-L soil heat flux plate	5%	Energy Fluxes calculations
Subsurface Moisture Content	EC-5 Probe	0.03 $m^3 m^{-3}$	Energy fluxes calculations

Section S2 - Derivation of the observed energy balance

S2.1 Derivation of soil water content and mass fractions

Measured soil water content from the in-situ soil moisture probes was not used, as its temporal response to rainfall was found to be unreliable. Instead, soil water content was derived from the mass of water in the substrate, estimated from lysimeter data.

The water mass at field capacity ($m_{w,fc}$) was first calculated as:

$$m_{w,fc} = VWC_{fc} * V_T * \mu_w \quad \text{(S1)}$$

Where VWC_{fc} is the volumetric water content at field capacity (from Sims, 2016 who performed detailed water balance assessments of the same roof), V_T is the total volume of soil and μ_w is the water density. The dry mass of the module at field capacity ($m_{d,fc}$) was then obtained as:

$$m_{d,fc} = m_{T,fc} - m_{w,fc} \quad \text{(S2)}$$

where $m_{T,fc}$ is the total mass at field capacity. Assuming the dry mass remains constant, the water mass at each timestep was calculated as:

$$m_w = m_T - m_d \quad \text{(S3)}$$

where m denotes mass, and the subscripts w, T and d, represent water, total and dry respectively. Once the mass of water is known it was converted to volume of water (v_w) as:

$$v_w = \frac{m_w}{\mu_w} \quad \text{(S4)}$$

The volumetric water content (*VWC*) was then calculated as:

$$VWC = \frac{v_w}{v_T} \quad \text{(S5)}$$

where v_T is the total volume. The corresponding mass fractions (solids: X_s and water: X_w) were derived as:

$$X_w = \frac{m_w}{m_T} \quad \text{(S6)}$$

$$X_s = 1 - X_w \quad \text{(S7)}$$

The solids fraction was then partitioned into organic (X_o) and mineral (X_m) components, based on the assumption that organic matter constitutes 6% of the dry mass (Perelli, 2014):

$$X_o = X_s * 0.06 \quad \text{(S8)}$$

$$X_m = X_s - X_o \quad \text{(S9)}$$

S2.2 Derivation of the volumetric heat capacity

To account for variations in soil thermal properties with changes in moisture and composition, the volumetric heat capacity (C_v) of the substrate was calculated as a mass-weighted sum of the specific heat capacities (*C*) of its components, multiplied by the bulk density (ρ_b):

$$C_v = \rho_b(X_m C_m + X_w C_w + X_o C_o) \quad \text{(S10)}$$

This formulation allows $C_v$to vary dynamically with soil water content, improving the accuracy of soil heat flux calculations.

S2.3 Derivation of latent heat flux, soil heat flux and surface temperature

The processed and derived variables provided the basis for calculating the observed Q_e and Q_g. The latent heat flux is calculated from the output of lysimeters using:

$$Q_e = \left[\frac{(P-d)+\Delta W}{\rho_w A}\right]\rho_w L_v \quad \text{(S11)}$$

where, P is precipitation, d is the drainage; ΔW is the weight loss of the modules due to evapotranspiration; ρ_w represents water density; A is the area of the module and L_v is the latent heat of vaporization, calculated from the measured air temperature.

Evapotranspiration was derived from the calibrated lysimeter signal, which was converted to absolute weight values. Changes in weight between consecutive timesteps were used to estimate water loss, assuming that under rain-free conditions, decreases in weight changes are solely due to evapotranspiration.

The soil heat flux is calculated as:

$$Q_g = Q_{g_z} + C_v\left(\frac{\Delta T}{\Delta t}\right)z \quad \text{(S12)}$$

where Q_{gz} is the ground heat flux measured at depth z; and the second term represents the heat storage in the layer of depth z above the heat flux plate (ΔQ_s): C_v is the volumetric soil heat capacity and $\Delta T/\Delta t$ is the measured change of substrate temperature T over the time step t in the layer.

These equations were applied to the full dataset to obtain the reference values for Q_e and Q_g, which were used for evaluating the models' outputs. Surface temperature was directly measured using an infrared radiometer; however, since this represents radiative temperature, a conversion was applied to obtain the kinetic surface temperature to match the temperature output by the models. This adjustment uses:

$$T_k = \sqrt[4]{\left(\frac{\sigma {T_r}^4 - (1-\varepsilon)L_{\downarrow}}{\varepsilon\sigma}\right)} \quad \text{(S13)}$$

where T_k is kinetic temperature, σ is the Stefan Boltzmann constant, T_r is the radiative temperature, ε is the emissivity and $L_{\downarrow}$ is the incoming longwave radiation.

Section S3 – Propagation of observed uncertainties

As with any field dataset, the measurements used in this study are subject to uncertainties. These arise from instrument precision, calibration, environmental noise, data processing, and, in some

cases, the need to estimate variables that are not directly measured. In this study, observations are treated as the reference against which model performance is assessed; however, their associated uncertainties were quantified following the error-propagation framework of Taylor (1997). Uncertainties were explicitly evaluated for the Q_e and Q_g.

S3.1 Uncertainty in Q_e

Based on Eq. (S11), Q_e depends on precipitation, drainage, and the change in module weight. L_v and module area are treated as constants; the uncertainty in L_v is negligible relative to the mass-related terms, and A is known exactly. The uncertainty therefore propagates through the mass term (S):

$$S = P - d + \Delta W \tag{S14}$$

Assuming small and independent errors, the absolute uncertainty in S is:

$$\sigma_S^2 = \sigma_P^2 + \sigma_d^2 + \sigma_{\Delta W}^2 \tag{S15}$$

where the uncertainties of P and d are known, and since $\Delta W = W_1 - W_2$ its uncertainty is:

$$\sigma_{\Delta W}^2 = \sigma_{W1}^2 + \sigma_{W2}^2 \tag{S16}$$

where W_1 and W_2 are consecutive lysimeter measurements. The relative uncertainty in the mass term is:

$$\frac{\sigma S}{S} \tag{S17}$$

Because Q_e was computed separately for two lysimeters and then averaged, the relative uncertainty was first calculated for each lysimeter and then combined as the average uncertainty of the two independent estimates.

S3.2 Uncertainty in Q_g

For this flux the uncertainty arises from the heat flux plate measurement (Q_{gz}), the soil heat storage term (ΔQ_s), and the uncertainties in bulk density, water content, and heat capacity that enter the calculation of ΔQ_s. The total uncertainty is:

$$\sigma_{Q_g}^2 = \sigma_{Q_{gz}}^2 + \sigma_{\Delta Q_s}^2 \quad \text{(S18)}$$

where plate uncertainties follow manufacturer specifications and applying Taylor's propagation rule to the storage term equation, given by Eq. (S13), we have:

$$\sigma_{\Delta Q_s} = z\sqrt{\left(\frac{\Delta T}{\Delta t}\right)^2 \sigma_{C_v}^2 + \left(\frac{C_v}{\Delta t}\right)^2 \sigma_{\Delta T}^2} \quad \text{(S19)}$$

where $\sigma\Delta T$ is given by the sum in quadrature of the instrument measurement error.

S3.3 Uncertainty in the volumetric heat capacity

Heat capacity is expressed as:

$$C_v = \rho_b S\,(X_w) \quad \text{(S20)}$$

where $\rho_b$is bulk density and $S(X_w)$is the weighted heat capacity of the constituents, written as:

$$S(X_w) = X_w C_w + (1 - X_w)(0.06C_o + 0.94C_m) \quad \text{(S21)}$$

Only $\rho_b$and $X_w$carry uncertainty; heat capacities are treated as constants. Given that C_v is the product of ρ_b and S, the relative uncertainty is:

$$\left(\frac{\sigma_{C_v}}{C_v}\right)^2 = \left(\frac{\sigma_{\rho_b}}{\rho_b}\right)^2 + \left(\frac{\sigma_S}{S}\right)^2 \quad \text{(S22)}$$

The sensitivity of S to changes in water fraction is:

$$\frac{dS}{dX_w} = C_w - C_{solids} \quad \text{(S23)}$$

where $C_{solids} = 0.06C_o + 0.94C_m$. Thus:

$$\sigma S = |C_w - C_{solids}|\sigma X_w \quad \text{(S24)}$$

S3.4 Uncertainty in the water fraction (X_w)

For each lysimeter, the water mass fraction $X_w$was computed from the dry mass at field capacity (m_d) and the total module mass at a given time step (m_T) as:

$$X_w = 1 - \frac{m_d}{m_T} \quad \text{(S25)}$$

Both m_d and m_T are subject to uncertainty due to the resolution and accuracy of the lysimeter load cells. Treating these errors as small and independent, and applying the standard error-propagation, the uncertainty in X_w is:

$$\sigma_{X_w}^2 = \left(\frac{m_d}{m_T^2}\right)^2 \sigma_{m_T}^2 + \left(\frac{1}{m_T}\right)^2 \sigma_{m_d}^2 \quad \text{(S26)}$$

where σ_{m_T} and σ_{m_d} are the absolute uncertainties in total mass and dry mass, respectively.

Water content was derived independently for the two lysimeters used in the study, and the value used in the heat-capacity calculation is the mean of these two estimates.

Section S4 – Summary of observed uncertainties

The mean daytime uncertainties for Q_e, Q_g, C_v, and X_w are summarized in Table S2. For Q_e, the dominant source of uncertainty is the change in lysimeter weight (ΔW). Although the lysimeters are highly sensitive, the hourly mass differences are frequently smaller than the instrument's absolute uncertainty, which results in large relative uncertainties for many hours. To avoid including unrealistically noisy estimates, Q_e values were retained only when the relative uncertainty of the mass term ($\sigma S/S$) was below $3\sigma\Delta W$ for both lysimeters; otherwise the hour was classified as "not reliable."

For Q_g, uncertainty arises from the heat-flux plate measurement and from the soil heat-storage term (ΔQ_s). The uncertainty in ΔQ_s depends on uncertainties in C_v and in the soil temperature difference ΔT. The uncertainty in C_v is comparatively small (mean relative uncertainty 1.5%), as it is driven mainly by uncertainties in bulk density and in the water mass fraction X_w. The uncertainty in X_w itself is on the order of 3×10^{-4} (absolute), reflecting the high precision of the lysimeters relative to the total module mass. While these propagate into ΔQ_s, their contribution is minor compared with ΔT uncertainty.

Table S2: Uncertainties in the observed data

Variable	Mean uncertainty	Unit of measure
Q_e	39	W m^{-2}
Q_g	14	W m^{-2}
C_v	16594	J m^{-3} K^{-1}
X_w	0.0003	N/A

Section S5 - Models' input parameters and initialization

The input parameters—and initial values and sources—required for each model are defined in Table S3. The models require a single value for each parameter. Some parameters, such as albedo, absorptance, LAI, plant height, and specific heat, can vary over time. However, a complete time series for these parameters was not available (except for albedo), as they were measured only on specific dates as part of other studies conducted on the green roof. For initializing the model, appropriate values for the specific time of the season were used, based on the available measurements and previous studies on the green roof.

Table S3: Model input parameters

	Parameter	Model	Initial Value	Source
Vegetation	Type of vegetation	WRF-MLGR	*Sedum Spurium*	-
	Leaf area index (LAI)	Both	2-3.7	Estimated from Sia (2016)
	Albedo	Both	0.15 – 0.25	Measured
	Emissivity	Both	0.96	(Kurukulaarachchi, 2017)
	Min. stomatal resistance (MSR) (s m^{-1})	Both	500	Calibrated, based on ranges provided by Piccinini Scolaro et al. (2024) and Tabares-Velasco and Srebric (2012)

	Max. stomatal resistance (s m^{-1})	WRF-MLGR	1125	(Zhao et al., 2014)
	Roughness length for momentum (m)	Both	0.01	(De Munck et al., 2013)
	Height of plants (m)	ER	0.087 – 0.159	Estimated from Tran et al. (2019)
Soil (loam – sandy loam growth media)	Number of layers and thickness (m)	Both	ER: Two, top (0.07) and root layer (0.08) WRF: detailed on Table 3.5	-
	Dry soil thermal conductivity (W m^{-1} K^{-1})	ER	0.194	(Perelli, 2014)
	Porosity (m^3 m^{-3})	Both	0.45	(Perelli, 2014)
	Dry bulk density of the growing media (kg m^{-3})	ER	751.80	Measured
	Specific heat capacity (J kg^{-1} K^{-1})	ER	1052	Estimated by back-calculation
	Saturated hydraulic conductivity (m s^{-1})	ER	1.67×10^{-4}	(Perelli, 2014)
	Soil suction (m)	WRF-MLGR	-0.1	Inferred from Perelli (2014)
	Dry soil heat capacity (J m^{-3} K^{-1})	WRF-MLGR	8.03×10^{5}	(Perelli, 2014)
	Field capacity	WRF-MLGR	0.193	(Sims, 2016)
	Wilting point	WRF	0.05	Software Default value
	Absorptance (thermal/longwave)	WRF-MLGR	0.96	(Kurukulaarachchi, 2017)
	Absorptance (solar/shortwave)	WRF-MLGR	0.75 – 0.85	Inferred from measured albedo
	Absorptance (visible wavelength)	ER	0.7	Software Default value

The MSR parameter was calibrated to better represent the green roof system dynamics. We used an independent period not included in the main analysis for sensitivity testing. Values from 300 to 700 s m^{-1} were evaluated, with 500 s m^{-1} selected based on improved agreement between modeled and observed fluxes.

ER required initialization variables include: foliage temperature, soil surface temperature, soil temperature at depth z, soil temperature at depth z_2, water content for the two layers, albedo, current runoff, cumulative runoff, current evapotranspiration and cumulative evapotranspiration.

Foliage temperature is approximated by an air temperature measured within the canopy; soil surface temperature is represented by an air temperature measured near the soil surface, soil temperatures at depths z and z_2 were measured at 2.54 cm and 10.16 cm; the water content was calculated using the method outlined in Sect. S2. Since we do not have water content separated by layers, the same value was used for both layers; albedo was calculated as the full period average albedo using the measured incident and reflected shortwave radiation. Current runoff, cumulative runoff, current evapotranspiration and cumulative evapotranspiration were all set to zero for the initial time step.

In WRF-MLGR, temperature, water content and volumetric heat capacity must be initialized for each of the ten soil layers. For the four layers representing the built roof a temperature measured at the built roof surface was used. For the two deeper layers of the green roof the temperature measured at 10.16 cm is used, and for the four most superficial layers the temperature measured at 2.54 cm is used. As a result, the 15 cm substrate is represented by two soil layers instead of six, due to data limitations, since no additional measurements were available to characterize all six layers. Volumetric heat capacity is set for each of the built layers according to the material they are composed of, while for the six green roof soil layers the same value is used. The depth of each layer must also be specified. Details on the soil 10-layer structure are presented in Table S4.

Table S4: WRF-MLGR layers, where layer 1 is the deepest layer while layer 10 is the most superficial layer

Layer	Material	Depth (m)	Heat Capacity (J m^{-3} K^{-1})
10	Soil	0.025	Water content dependent

9	Soil	0.005	Water content dependent
8	Soil	0.01	Water content dependent
7	Soil	0.02	Water content dependent
6	Soil	0.04	Water content dependent
5	Soil	0.05	Water content dependent
4	Bitumen membrane	0.008	1.7×10^6
3	Wood fiber overlay board	0.002	$3. \times 10^5$
2	Polyisocyanurate foam board	0.076	28.8×10^3
1	Concrete	0.062	2.3×10^6

[1]The values for the built roof component were extracted from IESVE (2021)

Section S6 – Additional figures

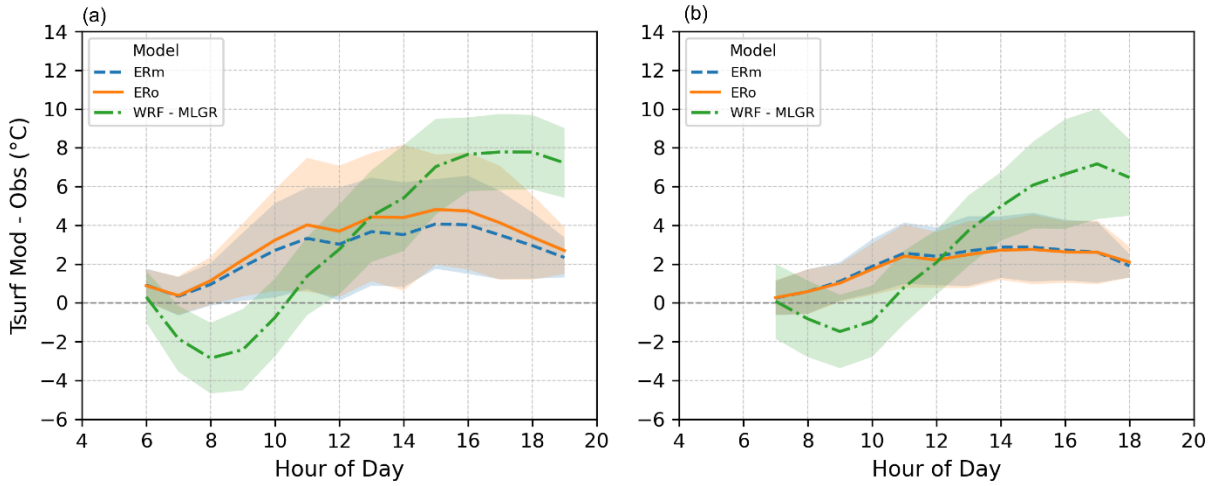

Figure S1: Hourly composite of the difference between modeled and observed T_{surf} for (a) the summer period and (b) the fall period.

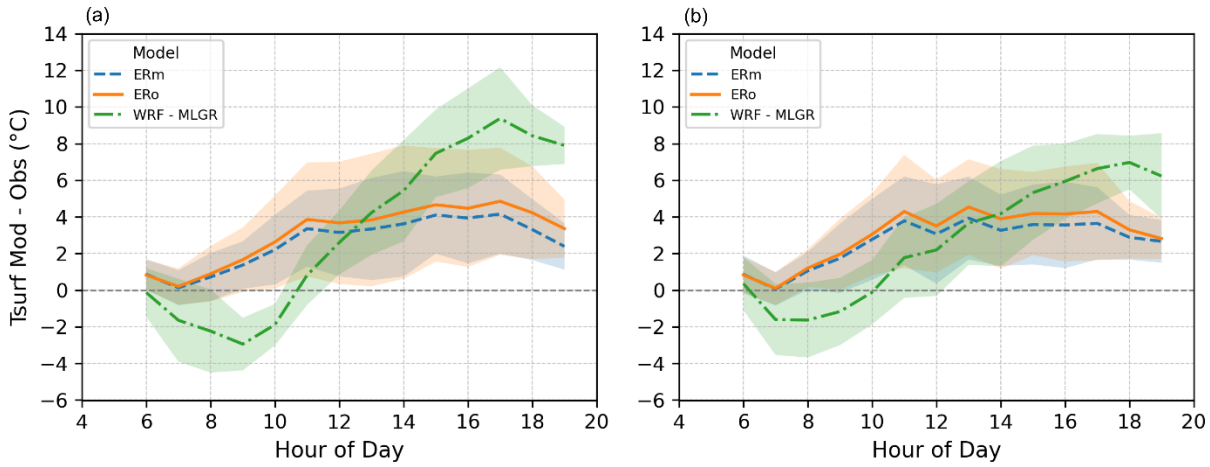

176

177 **Figure S2: Hourly composite of the difference between modeled and observed T_{surf} for a)**
178 **dry days and b) rainy days.**

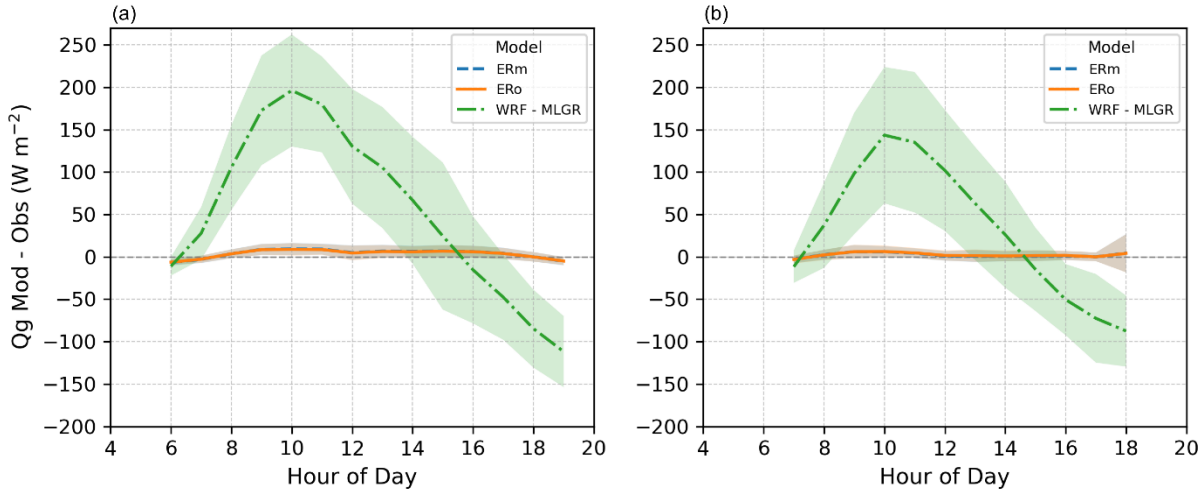

179

180 **Figure S3: Hourly composite of the difference between modeled and observed Q_g for a) the**
181 **summer period and b) the fall period.**

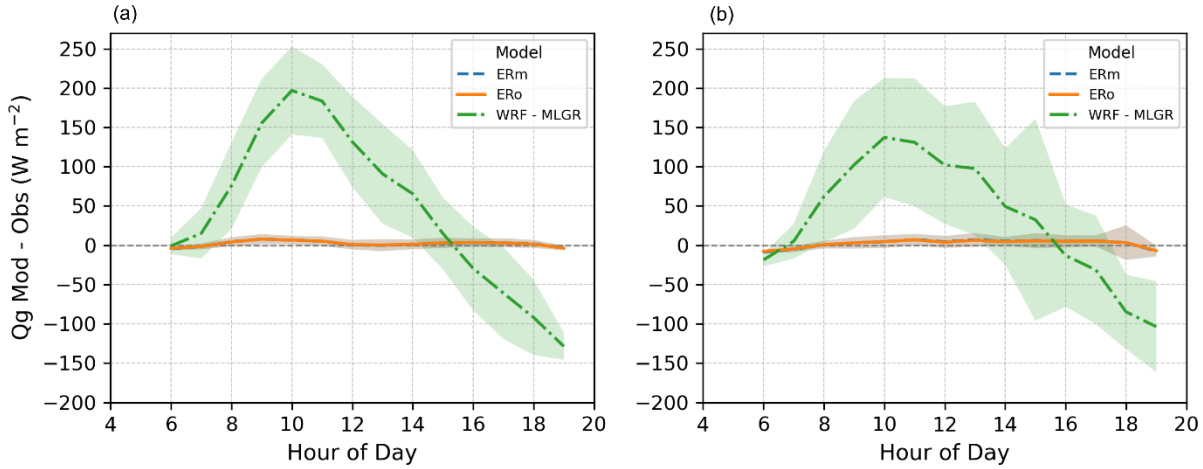

Figure S4: Hourly composite of the difference between modeled and observed Q_g for a) dry days and b) rainy days.

References

De Munck, C. S., Lemonsu, A., Bouzouidja, R., Masson, V., and Claverie, R.: The GREENROOF module (v7.3) for modelling green roof hydrological and energetic performances within TEB, Geosci. Model Dev., 6, 1941–1960, https://doi.org/10.5194/gmd-6-1941-2013, 2013.

Integrated Environmental Solutions Ltd. (IESVE): Integrated Environmental Solutions Ltd.: *Table 6 Thermal Conductivity, Specific Heat Capacity and Density*, IESVE Help Documentation, https://help.iesve.com/ve2021/table_6_thermal_conductivity__specific_heat_capacity_and_density.htm, 2021 (accessed April 2025)

Kurukulaarachchi, D. C.: Temporal Variability In The Daytime Green Roof Energy Balance During Drying Periods, MSc Thesis. The University of Western Ontario, https://hdl.handle.net/20.500.14721/27407, 2017.

Perelli, G. A.: Characterization of the Green Roof Growth Media, MSc Thesis. The University of Western Ontario, https://hdl.handle.net/20.500.14721/35037, 2014.

Piccinini Scolaro, T., Ghisi, E., and Silva, C. M.: Assessing the impact of evapotranspiration from green roofs on reducing surface temperatures, Journal of Building Engineering, 95, 110095, https://doi.org/10.1016/j.jobe.2024.110095, 2024.

Sia, M. E.: Evapotranspiration from extensive green roofs: influence of climatological conditions, vegetation type, and substrate depth, MSc Thesis. The University of Western Ontario, https://hdl.handle.net/20.500.14721/34186, 2016.

Sims, A. W.: Stormwater Management Performance of Green Roofs, MSc Thesis. The University of Western Ontario, https://hdl.handle.net/20.500.14721/35793, 2016.

206 Tabares-Velasco, P. C. and Srebric, J.: A heat transfer model for assessment of plant based roofing
207 systems in summer conditions, Building and Environment, 49, 310–323,
208 https://doi.org/10.1016/j.buildenv.2011.07.019, 2012.

209 Taylor: An Introduction to Error Analysis. The Study of Uncertainties in Physical Measurements.,
210 Second., University Science Books, California, 1997.

211 Tran, S., Lundholm, J. T., Staniec, M., Robinson, C. E., Smart, C. C., Voogt, J. A., and O'Carroll,
212 D. M.: Plant survival and growth on extensive green roofs: A distributed experiment in three
213 climate regions, Ecological Engineering, 127, 494–503,
214 https://doi.org/10.1016/j.ecoleng.2018.09.027, 2019.

215 Zhao, M., Tabares-Velasco, P. C., Srebric, J., Komarneni, S., and Berghage, R.: Effects of plant
216 and substrate selection on thermal performance of green roofs during the summer, Building and
217 Environment, 78, 199–211, https://doi.org/10.1016/j.buildenv.2014.02.011, 2014.

218